To appear in ANS Proceedings 1992 NHTC
Aug. 9-12, San Diego

FILM BOILING FROM SPHERES IN SINGLE- AND TWO-PHASE FLOW

C. Liu, T.G. Theofanous and W.W. Yuen
Center for Risk Studies and Safety
Department of Chemical and Nuclear Engineering
University of California, Santa Barbara
Santa Barbara, California 93106
Telephone (805) 893-4900

DOE/ER/12933--3

DE93 000887

ABSTRACT

Experimental data on film boiling heat transfer from single, inductively heated, spheres in single- and two-phase flow (saturated water and steam, respectively) are presented. In the single-phase-flow experiments water velocities ranged from 0.1 to 2.0 m/s; in the two-phase-flow experiments superficial water and steam velocities covered 0.1 to 0.6 m/s and 4 to 10 m/s, respectively. All experiments were run at atmospheric pressure and with sphere temperatures from 900 °C down to quenching. Limited interpretations of the single-phase-flow data are possible, but the two-phase-flow data are new and unique.

Nomenclature

C	specific heat
D	diameter
g	gravitational constant
h	heat transfer coefficient
h_{fg}	latent heat of evaporation
h'_{fg}	$=h_{fg}+0.68(T_p-T_s)C_v$
k	thermal conductivity
M	mass
q	heat flux
Q	volumetric heat source
t	time
T	temperature
U	velocity

Greek

ϵ	emissivity
μ	viscosity
ρ	density
σ	Stefan–Boltzman constant
χ	steam quality

subscripts

a	ambient condition
ℓ	liquid
p	(spherical) particle
s	saturation value
v	vapor

I. INTRODUCTION

This study is a part of a comprehensive experimental program aiming to establish the data base necessary for deriving the transfer (constitutive) laws necessary for closing the three-fluid model for general (transient, non-1D) systems in the disperse regime. Such models have been found useful[1,2] for establishing upper limits on the energetics of large-scale steam explosions—the mechanism is water depletion in the mixing zone. In the absence of experimental data, the initial computations were based on closures from extrapolations of two-phase formulations. On this basis, the emphasis in this program is on very high temperature spheres (where radiation is important), saturated coolant conditions (in single- or two-phase flow), a wide range of flow velocities, and a wide range of relative velocities and internal length scales in the steam-water flow. The latter aspect is to account for the widely variable, highly transient, two-phase flow regimes found within the mixing zone; the transient, typically of the order of 1 s, is referred to as premixing, a sequence of metastable states of interdispersed melt, water, and steam phases through which a steam explosion can propagate, given an adequate trigger.

The program includes heat transfer and drag measurements in single- and multi-particle array configurations. In addition to these fundamentally-oriented studies, a complementary experimental program on the integral aspects of such premixing transients is already in progress.[3] In this paper we consider only heat transfer from single spheres.

Regarding previous work, no data for a two-phase coolant could be located; for a single-phase coolant only the relatively recent work of Aziz et al.[4] could be identified as relevant. These data are based on transient cooling of nickel-plated copper spheres, 10 and 20 mm in diameter, from initial temperatures of ~500 °C (475 and 513 °C). The spheres were forced to sink in a 20-cm-deep water pool at velocities up to 1.8 m/s (0.1 m/s seems to be the minimum velocity used). In addition, Aziz et al.[4] extended and unified the theories of Frederking and Clark,[5] of Witte,[6] and of Witte and Orozco[7] by including buoyancy and pressure forces (parabolic profile) on the vapor film, as well as radiation. The predicted trends were consistent with their experimental data, but quantitatively low by more than a factor of 2. This was attributed to the "large-amplitude waves observed on the vapor film, or any heat transfer in the separated wake region" not accounted for in the theory. At the relatively low sphere temperatures in these tests, the radiation component to the total heat transfer was negligible.

The result of the theory of Aziz is not available in closed form. For convenience, we can cite the limited cases

of Frederking and Clark[5] for pool boiling,

$$q = 0.586 \left\{ \frac{h_{fg} g k_v^3 \rho_v (\rho_\ell - \rho_v)}{D \mu_v (T_p - T_s)} \right\}^{1/4} (T_p - T_s) \qquad (1)$$

and of Witte[6] for forced convection boiling [an extension of the well-known results of Bromley et al.[8] for cylinders]

$$q = 2.98 \left\{ \frac{k_v \rho_v U_\ell h'_{fg}}{D(T_p - T_s)} \right\}^{1/2} (T_p - T_s) \qquad (2)$$

It is remarkable that the constant in this equation is by a factor of 4.2 higher than the theoretical value obtained by Witte—this need for a larger magnification (as compared to that needed by Aziz, as mentioned above) is probably the result of ignoring the parabolic profile in the vapor and buoyancy.

II. EXPERIMENTAL APPROACH

The present emphasis on widely varying but well-defined two-phase (coolant) flow conditions requires operation in a steady regime. This, in turn, requires an adequate and well-controlled heat supply to balance the losses at each operating point, including the extremely high-temperature range desirable for our present purposes. This is a very significant experimental challenge, as noted by Witte and Orozco.[7] These investigators met it by convectively heating the inside of a large, hollow copper sphere, thus limiting them to low temperatures (use of a refrigerant as coolant) and to a sphere support that virtually eliminated the downstream hemisphere. This solution is clearly not acceptable for our purposes, and after extensive experimentation using various alternatives, we selected the induction-heating method. Eventually, it became possible to instrument metallic spheres and to achieve a wide range of heating/cooling conditions without undue internal temperature gradients. The other major development was a two-phase flow mixer to conveniently and accurately provide a wide range of steam-water flow characteristics. The coolant loop, the two-phase mixer, and the instrumented test spheres are described in the rest of this section.

The Flow Loop is schematically illustrated in Figure 1. The arrangement of the mixer/test-section assembly is reversible such that they can be connected to the "top separator" or "water tank" which also serves as a separator in the down-flow arrangement. The down-flow geometry is more suitable to low-velocity two-phase flows, while the up-flow geometry is necessary for single-phase flow (no bubble interference) and it provides another experimental dimension for very high velocity two-phase flows. Water is recirculated with a pump and it is thermostatically maintained to a fixed temperature. The air or steam are supplied from the lab lines, filtered, metered and used in a once-through fashion, i.e. vented to the atmosphere or to a condenser after separation. These supply lines are equipped with heaters to heat the air, and droplet separators to "dry" the steam as necessary. All flow measurements are made with venturis with an expected accuracy of ~4%. An independent calorimetric check on the steam flow gave agreement to within 5%. With the exception of the mixer and test section, all loop components are externally insulated. In the present arrangement the loop is designed to a pressure of 10 bar, a maximum liquid flow of 100 GPM and a peak steam supply (at 5 bar) of 10 gram/s.

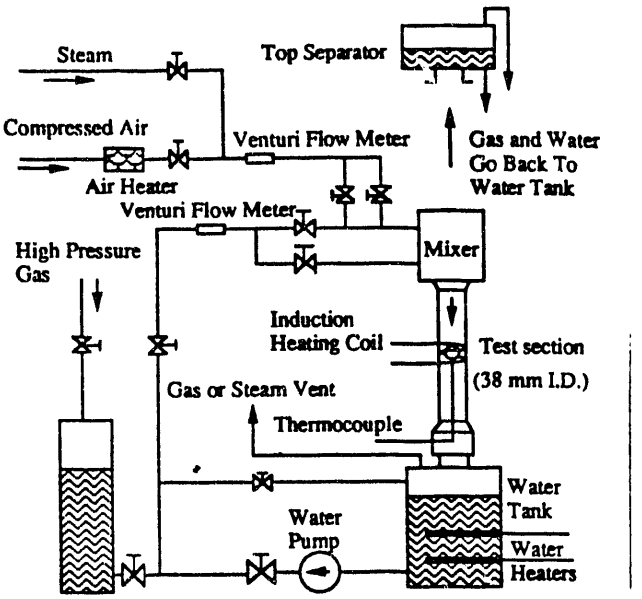

Fig. 1. Schematic of the flow loop.

The Two-Phase Mixer is schematically illustrated in Figure 2. The mixing is achieved by flowing one phase through the "needles" and the other through the annular spaces formed between the needle tips and the holes on a perforated plate. The needle assembly can be traversed such that the tip's position in relation to the plate/hole thickness can be adjusted to obtain different flow regimes. This arrangement is also reversible with water running through the needles and steam through the orifices and vice-versa.

The Test Section is shown in Figure 1. It consists of a pyrex tube 38 mm in diameter and 30 cm long; with the present pumping power, velocities up to 4 m/s can be obtained in it. The test sphere is supported from an end-flange to the test section, as shown in Figure 3; its distance from the other end of the test section (coolant entrance) is 170 mm (or 4.5 diameters). For the experiments reported here, we have used 9.5 mm stainless steel (type 316) balls, selected after extensive tests with various materials. The spheres are drilled, as shown in Figure 4, to accept thermocouples (stainless steel sheated, K type, 0.5 mm in diameter) at three positions: the forward stagnation point, the center, and the backward stagnation point—these are referred to as positions 1, 2 and 3, respectively. The sphere itself and the thermocouple sheaths provide adequate shielding from the RF electromagnetic field to allow undisturbed thermocouple signals, even during heating. Having established the limits of internal gradients with the three thermocouples, we have also used spheres with single thermocouples (1 or 2 positions) to confirm that heat losses through the supports are negligible. As shown in Figure 3, approximately 1.5 cm from the sphere, the thermocouple stems are reinforced by a ceramic tube leading to the main steel support off the flange. This steel support is equipped with a system of strain gauges (see Figure 3) for measuring the forces/drag. The test section (47 mm outer diameter) is wound, tightly, by 12 turns of 4.5 mm in diameter copper coil hooked up to an RF power supply [Lepel T-2.5-I-KCI-BW (T)] capable of supplying a peak of 2.5 kw induction power at 250–800 kHz.

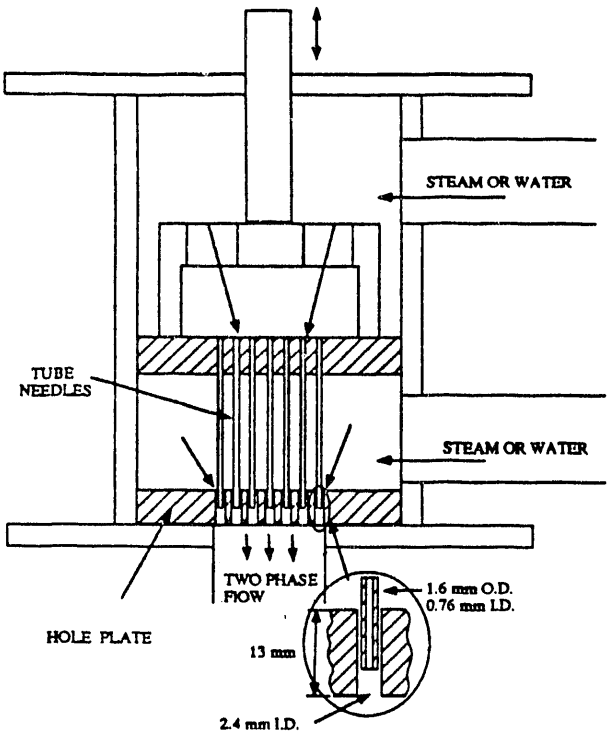

Fig. 2. Schematic illustration of the two-phase mixer (not to scale). The holes (69 total) are on a square grid of 4 mm center-to-center.

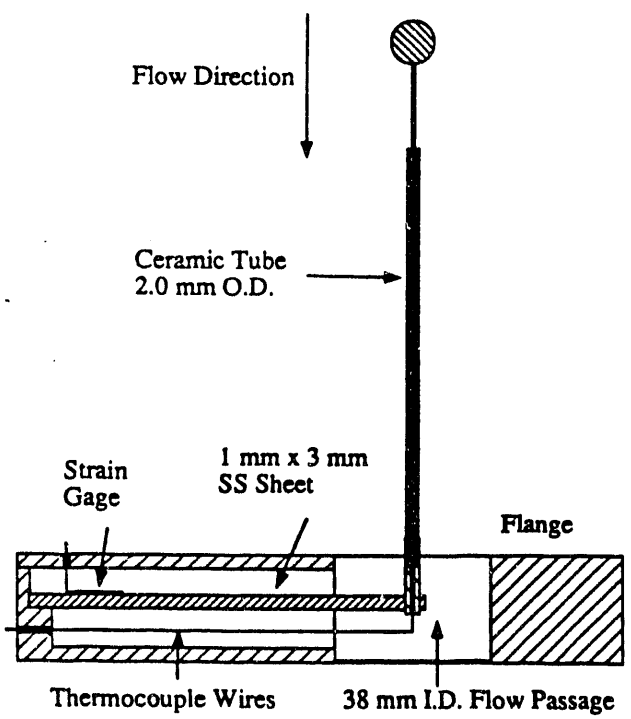

Fig. 3. The test sphere supported from the test section end flange.

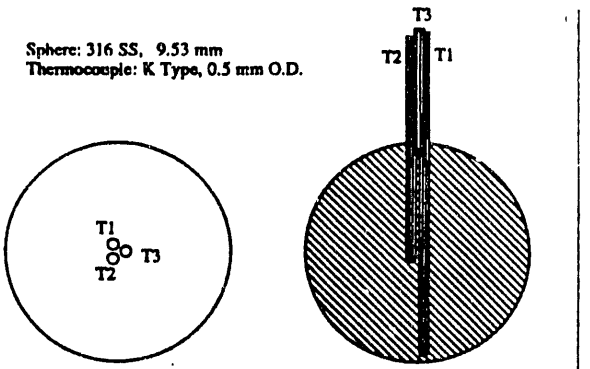

Fig. 4. Schematic of the instrumented test sphere.

III. EXPERIMENTAL PROCEDURES, CALIBRATIONS AND DATA REDUCTION TECHNIQUES

The main mode of operation, in this work, is to follow the transient cooldown from a well-established, initially, steady-state. The instantaneous heat fluxes can be deduced from an energy balance on the sphere, and the results do not depend on the calibration of the induction power supply. In this manner, from a single cooldown transient, we can obtain a very large number of data pairs, heat fluxes at respective sphere temperatures, between the initial and the final (quenched) states.

Besides this transient mode, it appeared interesting to also obtain data at steady-state, which is also possible in the present experimental arrangement. In particular, this totally independent technique (both in terms of the system thermal states, and the parameters that enter the data reduction) was expected to enhance the robustness of the data base generated in the transient mode. On the other hand, the anticipated drag measurements, in the future, require steady-state operation, and it appeared, therefore, important that the reliability of this mode be fully established at this time. This refers to the calibration of the power supply, which turned out not to be as straightforward as initially anticipated. Specifically, in the early stages of this work, we found that the presence of a water-continuous regime (single-phase runs) in the test section affected the power calibration obtained in air, in a rather unpredictable fashion. Eventually, we could relate this behavior to the electrical conductivity of the water—the discrepancy with the calibration in air diminished as the water conductivity was systematically increased, until it essentially disappeared at a conductivity of ~200 micromho. This is demonstrated by the data in the next section.

The calibration in the air was carried out as follows. With the test sphere in its usual position in the test section, the power was turned on and maintained at a given level until the sphere reached ~1000 °C, at which time the power was tripped (to zero)—this process was repeated at various power levels (indicated by the "plate current" meter on the power supply). A typical temperature transient is shown in Figure 5. From these data (recorded on a PC at a rate of 5 Hz) the power input could be obtained as a function of the sphere temperature as shown in Figure 6 (actually shown normalized by the sphere surface area). This involved differentiation of the temperature signals, carried out with a "local" sliding curve-fit to 5 consecutive readings, and use

in

$$Q = M_p C_p(T_p)\frac{dT_p}{dt} + h\pi D^2(T_p - T_\infty) + \epsilon\sigma\pi D^2(T_p^4 - T_a^4) \quad (3)$$

In the above equation, the heat capacity of 316 stainless steel given as a function of temperature[9] was used. The heat transfer coefficient was estimated from natural convection heat transfer,[10] and the corrected, by the heat losses, power is also shown in Figure 6. The emissivity (a value of 0.8 for "aged" spheres) was used to match the corrected power to zero for the whole cooldown period. From these results, a composite of calibration curves could be assembled as shown in Figure 7.

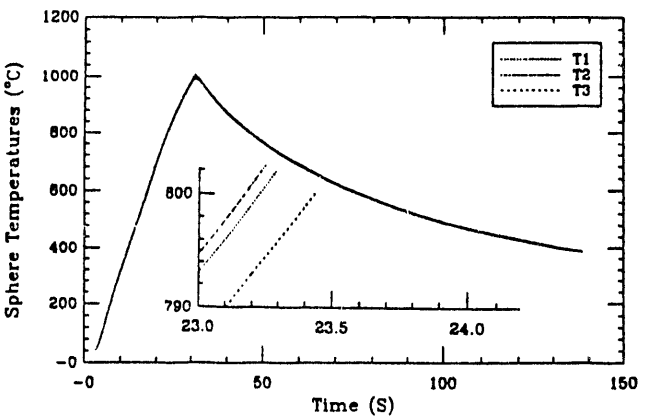

Fig. 5. A typical temperature transient during a calibration run in air. Plate current 0.6 A. The insert shows a magnified portion.

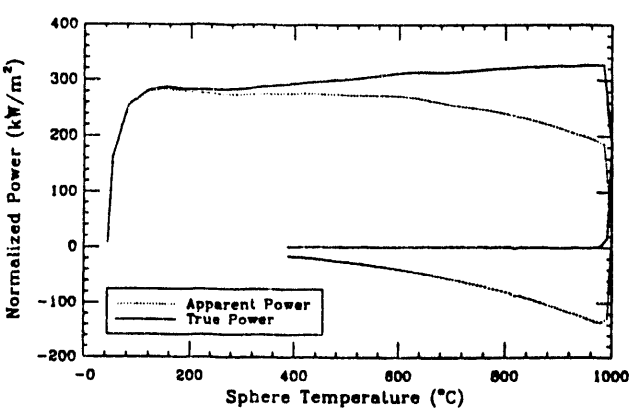

Fig. 6. The reduction of data in Figure 5, as described in the text.

Typical sets of primary experimental data obtained in single "runs" under the transient and steady-state modes of

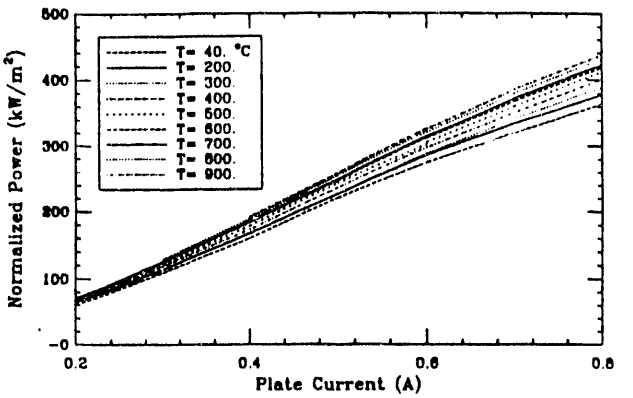

Fig. 7. Calibration (in air) of the power delivered to the sphere with its temperature as the parameter.

operation are shown in Figures 8 and 9, respectively. Figure 8 also shows the reduced heat flux transient obtained from

$$q = \frac{M_p C_p(T_p)}{\pi D^2}\frac{dT_p}{dt} \quad (4)$$

while the heat flux levels at each plateau of Figure 9 can be obtained from the respective plate currents (they are read to within 2%) in conjunction with the calibration in Figure 7.

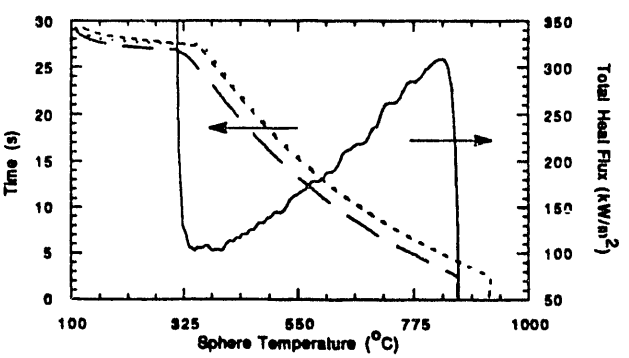

Fig. 8. Measured sphere temperature transients, and implied heat flux transients, in a transient mode run.

All the data were reduced to heat-transfer coefficients, and they are presented in terms of Nusselt numbers. For this purpose, the radiation contributions were subtracted out (by the usual 7/8 factor of Bromley), and the steam thermal conductivity, in the Nusselt number, was taken at saturation conditions. This is contrary to the usual approach of reporting total (including radiation) Nusselt numbers, as in Aziz et al.,[4] and using the "film" properties, as for example in Eqs. (1) and (2), but we have found that with these choices the deduced heat transfer coefficients are rendered *independent of the sphere temperature* (which in the present experiments ranged up to 900 °C), for all run conditions, thus allowing a more economical graphical representation.

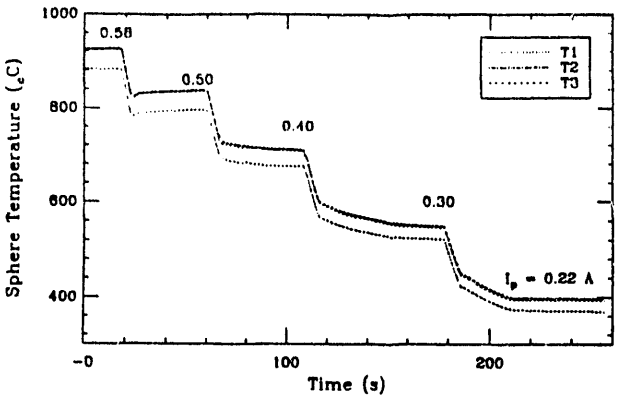

Fig. 9. Temperatures recorded in a run made in the steady-state mode. Each plateau provides a steady-state measurement.

However, whether there is a deeper implication here remains to be seen.

IV. EXPERIMENTAL RESULTS AND INTERPRETATIONS

A total of three sets of experiments were carried out. The first, referred to as "single-phase" runs, involved an all-liquid condition in upflow. The second set, referred to as "water–spray" runs, involved water-only in downflow and a coarse spray-like pattern generated by the water flowing through the perforated plate of the mixer. Finally, the third set, referred to as "two-phase" runs involved simultaneous water (through the plate holes) and steam (through the needles) flow, again in the downward direction, with the needle tips positioned half-way in the holes of the plate (see Figure 2). Each set of runs is discussed separately below.

Single-Phase Runs

In the transient mode, data were obtained with distilled water, deionized water, and tap water. Also, runs were made with the sphere at different stages of oxidation, including essentially metallic, slightly oxidized but still mostly metallic in appearance, well oxidized (black, but smooth), and heavily oxidized and corroded. In each case, the emissivity was measured (by the calibration procedure already described) and found to gradually progress from 0.5–0.6 to 0.8–0.9 through these four stages of oxidation. The last stage was obtained with prolonged use in highly conductive (conductivity over 100 micromho) tap water.

The results are presented in Figures 10 through 12, and as mentioned already, they include sphere temperature levels up to 900 °C. Figure 10 shows that with all these variations the data are contained within a ±15% band. The transition to the forced-convection regime, at a Re $\sim 10^4$ is also clearly exhibited. Figures 11 and 12 are in the form suggested by Eq. (2), and they confirm this asymptoric regime for water velocities about ~0.75 m/s; this corresponds to a Froude number $(U/\sqrt{gD})$ of ~2.45, which is in excellent agreement with that found by Bromley et al.[8] for cylinders. Some additional data in Figure 12 contrast the two extreme conditions of "distilled water/unoxidized ball" and "tap water/heavily oxidized and corroded ball," but even here the data expand only slightly then the band in Figure 11.

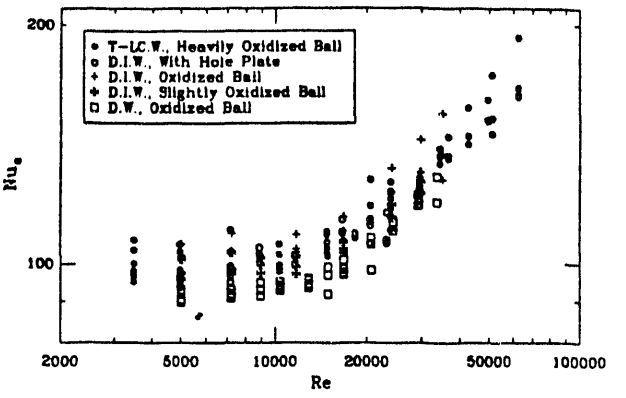

Fig. 10. Data from the single-phase set of runs. T-LC.W. is for tap, low conductivity (60 micromho) water; D.I.W. is for deionized water of similar conductivity; and D.W. is for distilled water.

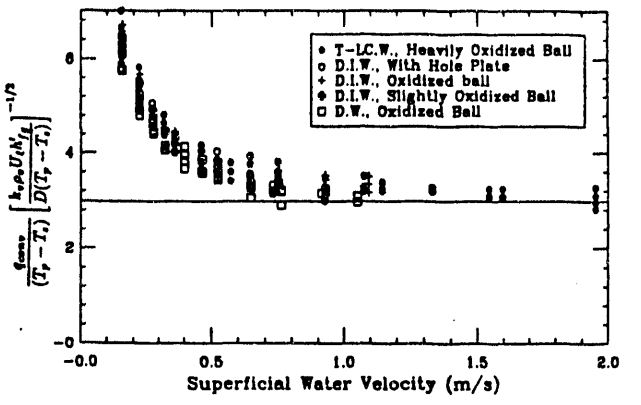

Fig. 11. The data of Figure 10, plotted in the form of Eq. (2).

Finally, the data obtained in the steady-state mode with systematically varying the water electrical conductivity are shown in Figure 13. By comparison to Figure 11, these data are seen to confirm the applicability of the power calibration (in air) to an all-water flow system, provided the electrical conductivity is adequately large (over 200 micromho). As already mentioned in the introduction, Aziz et al. have also presented one set of data for a sphere temperature of 475 °C (10 mm in diameter). These data were presented in the form of a total Nusselt number and using "film" properties as shown in Figure 14. Our data from the applicable runs to these conditions are shown to be in excellent agreement with these data of Aziz.

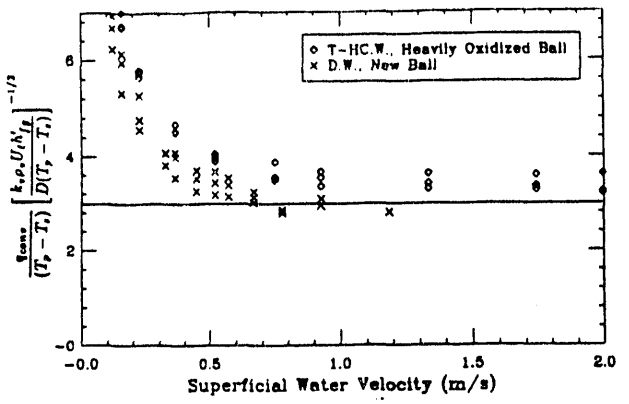

Fig. 12. Additional data for comparison with Figure 11. T-HC.W. is for tap, high conductivity (700 micromho) water.

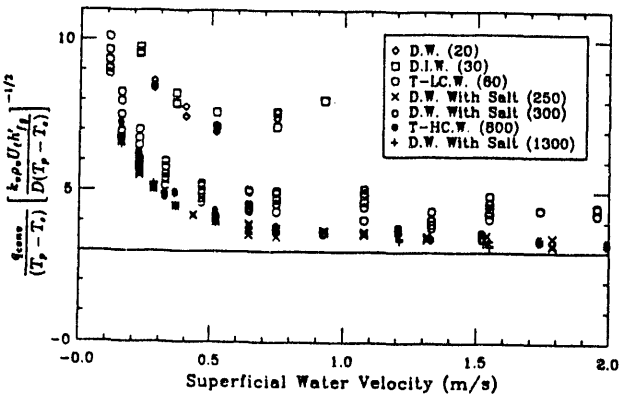

Fig. 13. The effect of water electrical conductivity (shown in parenthesis in micromho) on the power coupling to the sphere.

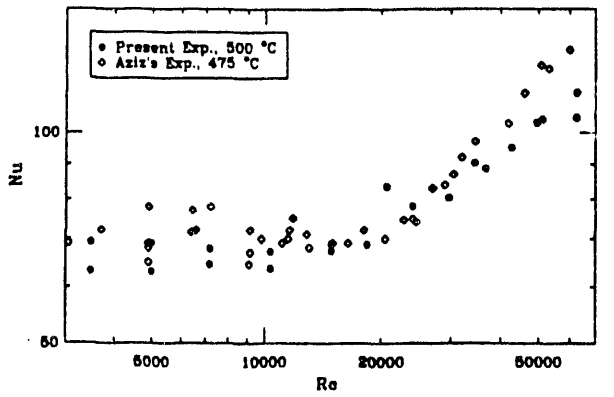

Fig. 14. Comparison of present experimental data with those presented by Aziz.

Water–Spray Runs

Within this set, runs were carried out at two positions of the needle tips—thus defining two subsets. In the first subset, the needle tips were completely removed from the plate holes, thus the water exited as 69 jets 2.4 mm in diameter. In the second subset, the needles were fully inserted (tips at the hole exits), thus the water emerged as circular jets (from the needles) surrounded by annular jets (from the spaces between the holes and the needles). The cylindrical jets had a diameter of 0.76 mm and the annular ones' inner and outer diameters were 1.6 and 2.4 mm, respectively. In both subsets of runs, the jets were seen to break up before impacting on the sphere; details are not known, but the above dimensions provide rough estimates of the characteristic water drop dimensions in the resulting "spray." Based on the sphere cross-sectional area, we estimate that roughly 6.3% of the coarse spray (about 4 to 5 "microstreams") impacted directly on the forward hemisphere of the ball. Most data were obtained in the transient mode, but a representative set of runs were also made in the steady-state mode, with the needle tips "in" (the second of the subsets discussed above).

The reduced results are shown in Figures 15 and 16 in terms of the inlet water jet velocity. All the data are

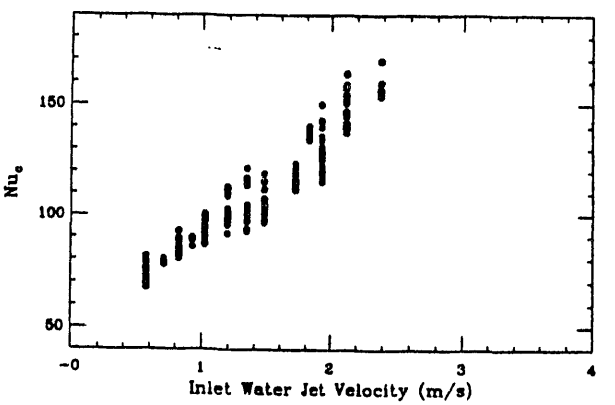

Fig. 15. Dependence of Nusselt number on water jet velocity. Needle tips out of configuration.

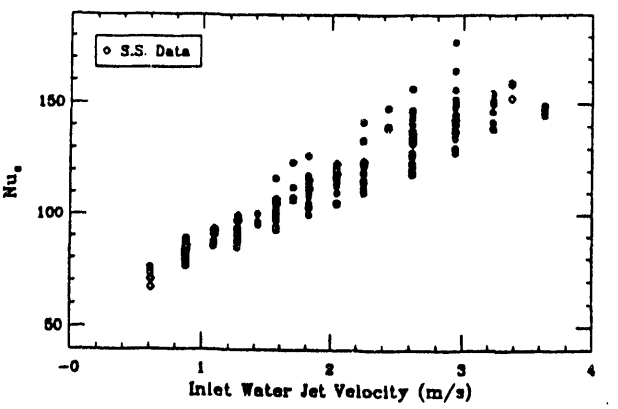

Fig. 16. Dependence of Nusselt number on water jet velocity. Needle tips in configuration.

clearly in the forced-convection regime, the two injection regimes agree at the low velocity end of the range investigated, but the two (linear) trends diverge as the water jet velocities increase, with the "needle-out" condition giving the higher values. Qualitatively, this is expected, because for the same jet velocity the "needle-out" condition (bigger area) yields a larger liquid volume fraction in the spray; however, quantitatively, no simple reduction (of this difference), by the liquid volume fractions, could be identified. The linear variation, with water velocity observed here, is in marked contrast to the square-root dependence found in the single-phase runs (see Figure 11). The theoretical basis for this key difference in behavior remains to be established. The steady-state data in Figure 16 are seen to be in good agreement with those obtained in the transient mode.

Two-Phase Runs

In this set, the inlet flow pattern was created as the annular liquid jets interacted with the "core" steam flow. This interaction initially took place within the exit hole plate of the two-phase mixer, as is made evident by the geometry in Figure 2, and it continued as the two streams flowed into the test section. Because of the high velocities, detailed observations of this interaction have not been possible so far; however, we expect extensive dispersion of the water jets to very fine spray, especially at the high steam velocities, which reached ~400 m/s (at the needle tips). The experimental runs were carried out in two subsets, and mostly in the transient mode. In the first subset, the steam flow rate was fixed at 4 different levels (152, 232, 304 and 376 m/s[a]), and the water velocity was changed to carry out each run. A set of steady-state data were also obtained for the steam velocity fixed at 304 m/s. In the second subset, the water velocity was fixed at 1.53 m/s, and various runs were made with steam velocities varying from ~150 m/s to ~400 m/s. The quality for any particular experimental condition can be obtained from the inlet steam and water jet velocities (U_v and U_ℓ) from

$$\chi \sim 1.12 \times 10^{-4} \frac{U_v}{U_\ell} \qquad (5)$$

The reduced data are presented in Figures 17 through 19. The consistency of data obtained in the transient and steady-state modes of operation is again clearly evident. Remarkably enough, that data obtained at the low level of steam velocity (152 m/s) are in very good agreement with those obtained in the water–spray set (no steam flow), see Figures 15 and 16. The effect of increased steam flow is evident in Figures 17 and 18, and it is even more clearly expressed by the data in Figure 19. Finally, from Figures 17 and 18, the linear dependence on water velocity is observed again, as in the water-spray runs; however, the slopes are now considerably lower.

V. CONCLUSIONS

1. A flexible experimental system, and a robust experimental technique are now available to test film boiling

[a] These steam velocities are estimates based on steam flow rate (saturated at 1 bar) and needle tip area. They are expected to be altered by the steam-water interactions within the "hole" space.

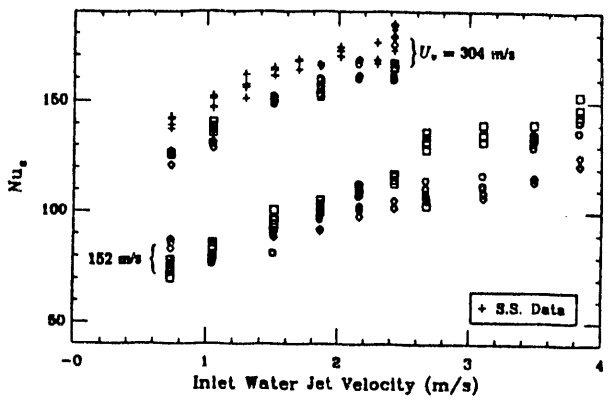

Fig. 17. Dependence of Nusselt number on water jet velocity for two fixed levels of steam flow. The steam jet velocities are indicated next to the corresponding data band. ○, □, ◇ indicate 3 different runs.

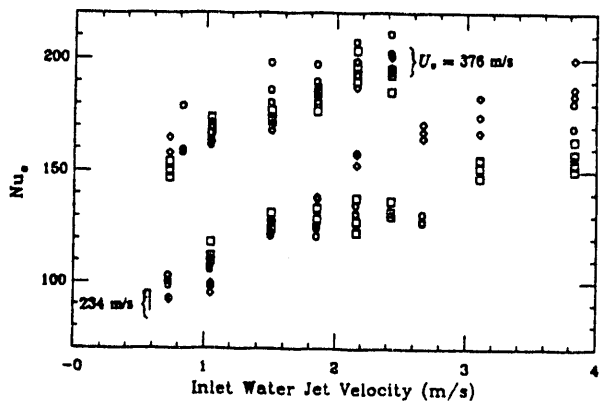

Fig. 18. Dependence of Nusselt number on water jet velocity for two fixed levels of steam flow. The steam jet velocities are indicated next to the corresponding data band. ○, □, ◇ indicate 3 different runs.

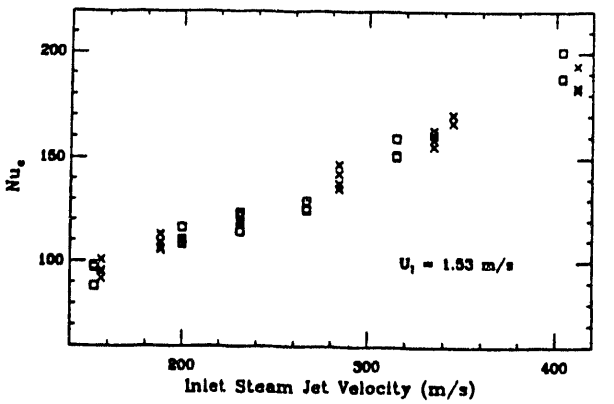

Fig. 19. Dependence of Nusselt number on inlet steam jet velocity, at a fixed water jet velocity (1.53 m/s). □, × indicate 2 different runs.

from very high-temperature single and multiparticle arrays of spheres in a wide variety of two-phase flows.

2. For single-phase flow, the forced convection regime sets in for velocities above 0.7 m/s (corresponding to a Froude number of 2.4, in good agreement with Bromley's results for cylinders) and it is described well with Eq. (2) proposed by Witte.[6]

3. For two-phase flows, the data show a strong effect of the velocity of the liquid phase (especially as it is accelerated by the vapor phase). Analytical interpretations need to be guided by additional data covering a wider range of conditions (in progress).

ACKNOWLEDGMENTS

This work is supported by the U.S. Department of Energy Grant No. DE-FG07-90ER12933. The able help of T. Salmassi and J. Beecher with experimental techniques is gratefully acknowledged.

REFERENCES

1. T.G. THEOFANOUS, B. NAJAFI and E. RUMBLE, "An Assessment of Steam-Explosion-Induced Containment Failure. Part I: Probabilistic Aspects," *Nuclear Science and Engineering* **97**, 259-281 (1987).

2. W.H. AMARASOORIYA and T.G. THEOFANOUS, "Premixing of Steam Explosions: A Three-Fluid Model," *Nuclear Engineering and Design* **126**, 23–39 (1991).

3. T.G. THEOFANOUS, S. ANGELINI, R. BUCKLES and W.W. YUEN, "On the Prediction of Steam Explosions Energetics," *Proceedings 19th Water Reactor Safety Information Meeting*, Bethesda, MD, October 24, 1991.

4. S. AZIZ, G.F. HEWITT and D.B.R. KENNING, "Heat Transfer Regimes in Forced-Convection Film Boiling on Spheres," *ANS Proceedings of the 23rd National Heat Transfer Conference*, 2149-2154 (1986).

5. T.H.K. FREDERKING and J.A. CLARK, *Advanced Cryog. Engng.* **8**, 501 (1963).

6. L.C. WITTE, *Ind. Eng. Chem. Fundamentals* **7**, 517 (1968)

7. L.C. WITTE and J. OROZCO, "The effect of Vapour Velocity Profile Shape on Flow Film Boiling from Submerged Bodies," *J. Heat Transfer* **106**, 191-197 (1984).

8. L.A. BROMLEY, N.R. LE ROY and J.A. ROBBERS, "Heat Transfer in Forced Convection Film Boiling," *Ind. & Eng. Chem.* **45**, 2639 (1953).

9. Y.S. TOULOUKIAN and E.H. BUYCO, "Specific Heat, Metallic Elements and Alloys," *Thermophysical Properties of Matter* **4**, IFI/Plenum, New York (1970).

10. T. YUGE, "Experiments on Heat Transfer from Spheres Including Combined Natural and Forced Convection," *J. Heat Transfer* ser. C **82**, 214 (1960).

DISCLAIMER

END

DATE FILMED

12/9/92